minerals

MDPI

Article

Sedimentary–Diagenetic Divergence Between Turbidite and Delta-Front Tight Sandstones: Chang 6 and Chang 8, Yuele Block, Southwestern Ordos Basin

Chi Li [1,*], Cheng Li [1], Yujie Bai [1], Xiaohui Zhang [1], Ling Xiao [2,3,4], Qingsi Pei [2,3,4] and Qinlian Wei [2,3,4,*]

[1] Research Institute of Exploration and Development, PetroChina Changqing Oilfield Company, Xi'an 710018, China; c8lc_cq@petrochina.com.cn (C.L.); byuj_cq@petrochina.com.cn (Y.B.)
[2] School of Earth Science and Engineering, Xi'an Petroleum University, Xi'an 710065, China; 13849736922@163.com (Q.P.)
[3] Shaanxi Key Laboratory of Petroleum Accumulation Geology, Xi'an Shiyou University, Xi'an 710065, China
[4] Key Laboratory of Intelligent Geophysical Exploration for Oil and Gas Resources of Shaanxi Higher Education Institutions, Xi' an 710065, China
* Correspondence: lichi_cq@petrochina.com.cn (C.L.); wql@xsyu.edu.cn (Q.W.)

Abstract

Turbidite sandstones of the Chang 6 member and delta-front sandstones of the Chang 8 member in the Yuele Block, southwestern Yishan Slope, Ordos Basin, serve as the primary tight oil reservoirs. In this study, a total of 243 continuous core samples from multiple wells were collected for integrated analyses, including cast thin-section observation, scanning electron microscopy (SEM), X-ray diffraction (XRD) of clay minerals, routine core physical property measurements and mercury intrusion porosimetry (MIP), to systematically compare sedimentary–diagenetic disparities between semi-deep lacustrine turbidites (Chang 6) and delta-front sandstones (Chang 8). Measured data indicate that the two intervals have similar average porosities of 9.27% and 9.88%, while their respective geometric mean permeabilities differ markedly, with values of only 0.142×10^{-3} μm^2 for Chang 6 and 0.260×10^{-3} μm^2 for Chang 8. Micro-pore-throat size and connectivity dominate reservoir fluid flow capacity, and total porosity alone cannot objectively evaluate reservoir quality. Delta-front sandstones of the Chang 8 member are supplied by a proximal magmatic-rich provenance from the southwest, and widespread grain-coating chlorite forms during early diagenesis, effectively mitigating compaction damage and inhibiting quartz overgrowth, leading to well-preserved primary pores. As mixed-provenance deposits lacking protective chlorite rims, Chang 6 turbidites experience more intensive compaction, and abundant fibrous illite and carbonate cements precipitate in the subsequent diagenetic stage to fill and separate pore throats, forming an isolated micropore network. Quantitative comparison with baseline parameters of the Longdong region reveals that the Yuele Block is located closer to the southwestern sediment source, resulting in higher contents of magmatic lithics and chlorite in Chang 8 as well as elevated illite concentrations in Chang 6 relative to regional averages, which verifies that source-to-sink transport distance regulates reservoir quality by driving the differentiation of clay mineral assemblages. A complete quantitative coupling sequence of "provenance supply–authigenic clay mineral-pore evolution" is defined herein, and two distinct sedimentary–diagenetic evolutionary routes are classified: high-quality delta-front reservoirs protected by grain-coating chlorite, and low-quality turbidite reservoirs blocked by illite–carbonate cements. This research refines the diagenetic differentiation rules for continental tight sandstones with diverse sedimentary origins in the Ordos Basin and provides quantitative mineralogical criteria for identifying tight oil sweet spots in proximal provenance blocks.

Check for updates

Academic Editor: Santanu Banerjee

Received: 30 June 2026
Revised: 27 July 2026
Accepted: 4 August 2026
Published: 11 August 2026

Copyright: © 2026 by the authors. Licensee MDPI, Basel, Switzerland. This article is an open access article distributed under the terms and conditions of the Creative Commons Attribution (CC BY) license.

Keywords: Ordos Basin; Yuele Block; Chang 6 turbidite tight sandstone; Chang 8 delta-front tight sandstone; reservoir characteristics; sedimentation; diagenesis

1. Introduction

The progressive depletion of conventional hydrocarbon reserves has accelerated exploration toward unconventional resource plays, among which tight oil is regarded as a potential route for reserve growth and production enhancement [1,2]. Lacustrine tight sandstone reservoirs represent a dominant unconventional hydrocarbon reservoir type in terrestrial sedimentary basins worldwide, yet their strong heterogeneity and complex diagenetic modification mechanisms lead to highly variable reservoir quality across different basins and blocks, restricting the establishment of universal geological prediction models.

In China, the Triassic Yanchang Formation within the Ordos Basin—the country's second-largest continental sedimentary depression—hosts substantial tight oil accumulations, with recent exploration successes in the southern basin underscoring the high demand for a process-based understanding of reservoir quality in these tight sandstones [3,4].

Analogous tight sandstone reservoirs worldwide, including the Upper Cretaceous Mesaverde Group in the Rocky Mountains and the Jurassic tight gas sands of the Norwegian North Sea, demonstrate that reservoir quality is universally governed via the interplay of depositional facies, diagenetic overprinting, and pore-throat architecture [5–8]. Yet, the relative importance of each factor varies markedly between blocks, enabling block-to-block comparative analysis to distinguish regional generic controls from block-specific phenomena [9]. Despite the extensive case studies on tight reservoir diagenesis that have been carried out globally, most existing empirical models are highly site-specific. A generalized, systematic workflow linking sedimentary provenance, clay mineral evolution, and differential diagenetic modification remains poorly established, which limits the cross-basin applicability of current reservoir evaluation theories.

Within the Ordos Basin, previous studies have identified multiple diagenetic agents responsible for reservoir densification. In the Nanliang area, Xiao et al. (2017) stressed the role of hydromica cementation in degrading Chang 6 reservoir quality [10,11]. In the Longdong region, Liu et al. (2018) documented the combined effects of siliceous, carbonate, and clay mineral cements on permeability differentiation between the Chang 6 and Chang 8 members and proposed a corresponding pore-evolution model [12,13]. While these contributions have substantially advanced our knowledge of regional diagenetic patterns, two major limitations persist. First, sedimentary facies, diagenetic fluid compositions, and burial histories vary markedly across the basin's structural units, rendering the mechanisms established in one area not directly transferable to others [10,12]. Second, most existing investigations focus on regional-scale trends, while intra-block heterogeneities and the quantitative relationships between depositional parameters and diagenetic products remain poorly constrained.

The Yuele Area, situated in the southwestern Ordos Basin, represents a strategically important exploration block. However, systematic, fine-scale comparative investigations of reservoir characteristics and their primary controlling factors for the Chang 6 and Chang 8 members in this area remain conspicuously absent—a knowledge gap that hinders targeted investigation strategies and limits the wider applicability of existing diagenetic models.

To address this research gap, we conduct a high-resolution comparative analysis of Chang 6 and Chang 8 tight sandstones in the Yuele Block. Based on 243 multi-well core samples, we integrate cast thin-section observation, SEM, clay mineral XRD, MIP, routine core measurements and well logging data to: (1) document the petrologic features, pore categories and micro pore-throat architectures of both intervals; (2) quantify the

combined impacts of sedimentary processes and diagenesis on reservoir physical properties; (3) explain the link between sediment source conditions, clay mineral differentiation and disparate pore evolution caused by burial alteration.

The results can guide reservoir assessment for proximal-provenance tight oil plays within the Ordos Basin and offer comparative insights for other continental lacustrine tight sandstone reservoirs. Beyond supporting local tight oil exploration in the Yuele Block, this work also delivers a reusable analytical framework to evaluate reservoir quality in analogous terrestrial tight sandstone sequences.

2. Geological Setting

The Ordos Basin, situated in the western part of the North China Block, is a typical cratonic basin characterized by stable subsidence, torsional migration, and multi-cycle evolution [14]. Based on its geological record and current structural framework, the basin can be subdivided into six primary tectonic units: the Yimeng Uplift, the Western Margin Thrust Belt, the Tianhuan Depression, the Yishan Slope, the Jinxi Flexural Fold Belt, and the Weibei Uplift [15–17].

The Yuele Area is located in the southwestern Ordos Basin, tectonically situated on the southwestern Yishan Slope, with an exploration area of approximately 2650 km^2. The study interval comprises the Chang 6 and Chang 8 members of the Upper Triassic Yanchang Formation. The Chang 8 member was deposited in a delta-front environment, characterized by underwater distributary channels and mouth bars. In contrast, the Chang 6 member formed in a semi-deep to deep lacustrine facies, dominated by sandy debris-flow and turbidity-current deposits. These dissimilar sedimentary settings provide the basis for subsequent diagenetic divergence (Figure 1).

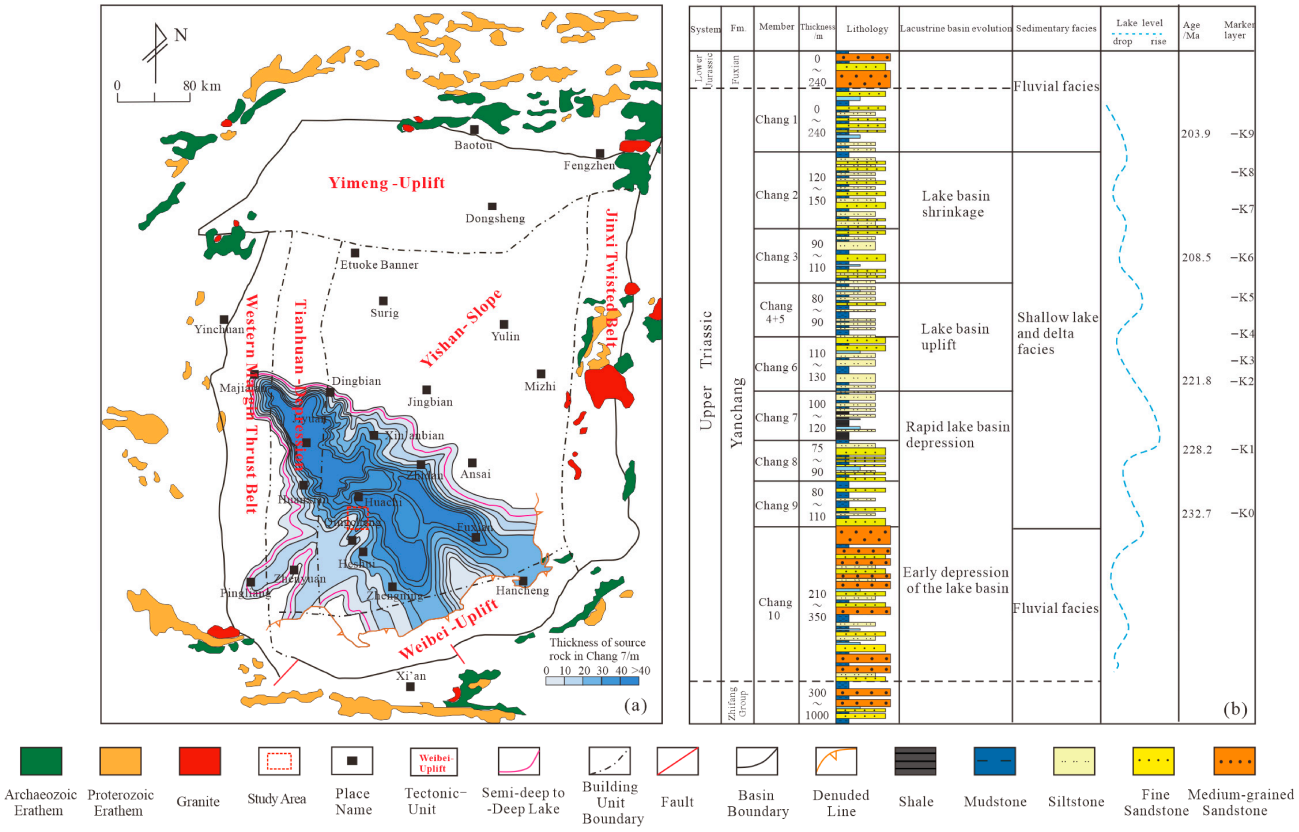


Figure 1. The geographical location of the study area and the lithological properties of the target layer. (**a**) structural characteristics and location of the study area in the Ordos Basin; (**b**) lithology characteristics column.

3. Methods

3.1. Study Area and Sampling

The Yuele Area is located in the southwestern Ordos Basin, tectonically situated on the southwestern Yishan Slope, with an exploration area of approximately 2650 km^2 (Figure 1). A total of 243 core plug samples were systematically collected from multiple wells covering the Chang 6 and Chang 8 members of the Yanchang Formation. Sampling ensured representation of different stratigraphic intervals and lithofacies. The precise well locations and sample depth intervals are available upon request.

3.2. Petrographic and Mineralogical Analysis

Standard thin sections with a thickness of 30 μm were prepared for all samples and stained with alizarin red S and potassium ferricyanide for carbonate minerals, aiming to distinguish calcite, ferroan calcite, and ankerite, as well as determine the mineral composition, cement types and their corresponding contents. Epoxy-impregnated thin sections were adopted to identify pore types under a Leica DM4500P petrographic microscope.

For SEM analysis, freshly broken rock chips (approx. 1 cm^3) were gold-coated and examined using a Zeiss EVO MA 15 scanning electron microscope operated at 15–20 kV. Energy-dispersive X-ray spectroscopy (EDS) was used to confirm clay mineral identifications.

Clay mineral assemblages and relative abundances were determined by X-ray diffraction (XRD) on oriented mounts of the <2 μm fraction, using a Bruker D8 Advance diffractometer with Cu-Kα radiation (40 kV, 40 mA). Quantitative estimates were derived from the integrated peak areas of glycolated samples, with an analytical error of approximately ±5% relative.

3.3. Physical Property Measurements

Porosity and permeability were measured for all 243 core plugs (1-inch diameter, 2–3 cm length) using a helium porosimeter (UltraPore-300) and a nitrogen permeameter (Temco PP-250), in accordance with Chinese oil and gas industry standards (SY/T 5336-2006) [18]. The relative measurement errors are generally <3% for porosity and <5% for permeability, based on repeated measurements of reference standards. Given the log-normal distribution typical of permeability in tight sandstones, both arithmetic and geometric means are reported; uncertainties are expressed as standard errors of the arithmetic mean.

3.4. Mercury Intrusion Porosimetry (MIP)

MIP was conducted on selected samples (n = 30) using a Micromeritics AutoPore IV 9520 instrument, with a maximum pressure of 207 MPa (30,000 psi), allowing for the detection of pore throats down to approximately 0.003 μm. Parameters calculated from the intrusion curves include: displacement pressure (Pd), median throat radius (R50), sorting coefficient, skewness, and mercury ejection efficiency. These parameters were calculated using standard geometric procedures.

3.5. Data Analysis and Reproducibility

All analytical procedures followed established laboratory protocols. Repeat analyses on duplicate samples indicate good reproducibility: for porosity and permeability, relative standard deviations (RSDs) are within 5%; for MIP parameters, RSDs are within 10%. The quantitative estimates of porosity loss due to compaction vs. cementation were derived from point-count data using the method of Houseknecht (1987) and Ehrenberg (1989) [19,20], assuming that primary porosity was initially at the Beard and Weyl (1973) [21] ideal value for well-sorted sands (approximately 47%). These estimates are inherently approximate and are interpreted as trends rather than absolute values.

4. Results

4.1. Petrological Characteristics

Thin-section observations show that the rock types of the Chang 6 member in the Yuele Area are mainly lithic feldspar sandstone and feldspar lithic sandstone, with little feldspar sandstone (Figure 2). All ternary plot data in this study adopt the international standard Q-F-L (quartz–feldspar–lithic fragment) ternary classification scheme. Notably, the statistical percentages of sandstone framework components for triangle plotting are calculated exclusively on the basis of framework grains (quartz, feldspar, and lithic fragments), with interstitial matrix and cement components excluded from statistics. The contents of quartz, feldspar, and lithic fragments are normalized to 100% to conform to the standard Q-F-L classification principle. The average quartz content is 33.96%, feldspar is 27.43%, and rock debris is 14.52%. Rock debris is dominated by metamorphic fragments (quartzite, phyllite, schist) and dolomite. Total interstitial material averages 17.45%, dominated by illite and iron calcite.

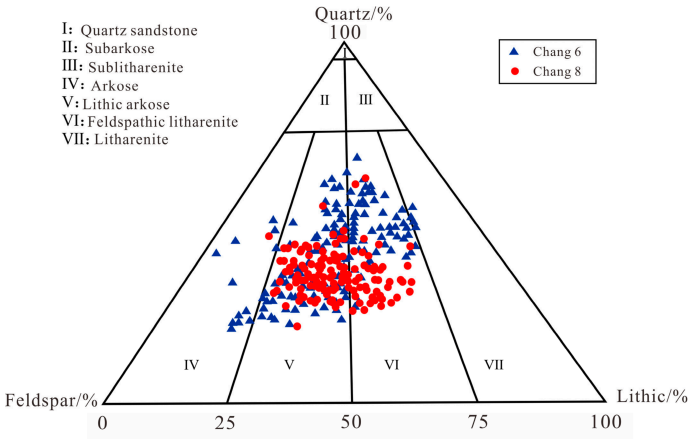


Figure 2. Rock type triangle of the Chang 6 member and Chang 8 member sandstone in the Yuele Area, Ordos Basin. (Q-F-L ternary classification; data are normalized to 100% based on framework grains only, excluding interstitial matrix and cements) (Folk, 1968) [21].

For the Chang 8 member, rock debris mainly consists of metamorphic and magmatic fragments (including eruptive rocks). Total interstitial material averages 16.42%, dominated by illite, chlorite, iron, calcite, and silica. In terms of composition, the Chang 6 member has higher quartz content than the Chang 8 member, but lower feldspar and rock debris contents (Figure 2 and Table 1). The relatively high magmatic lithics content (8.39%) in the Chang 8 Member provides a material basis for subsequent chlorite precipitation.

Table 1. Grain contents of the Chang 6 and Chang 8 members in the Yuele Area, Ordos Basin (grain content + matrix + cement + areal porosity = 100%. All parameters represent area fractions relative to the total thin-section field of view. Magmatic lithics, quartz and feldspar are subfractions of grain content.).

Member	Mineral Content (%)		Igneous Lithics (%)				Metamorphic Lithics (%)				Sedimentary Lithics (%)			Mica (%)	Sample Number
	Quartz	Feldspars	Granite	Extrusive Rock	Aphanitic Rock	High-Grade Metamorphic Rock	Quartzite	Schist	Phyllite	Metamorphic Sandstone	Chert	Limestone	Dolomite		
Chang 6	33.96	27.43	0.08	1.88	0.57	0.59	1.95	0.83	3.11	0.50	0.63	0.39	4.00	8.06	126
Chang 8	29.64	31.94	0.07	7.08	1.24	1.36	3.18	1.63	3.94	1.59	0.56	0.02	0.13	4.06	117

4.2. Physical Properties

Petrophysical statistical analysis of the Chang 6 and Chang 8 reservoirs is presented in Figure 3, which displays the frequency and cumulative frequency distributions of porosity and permeability for the two intervals.

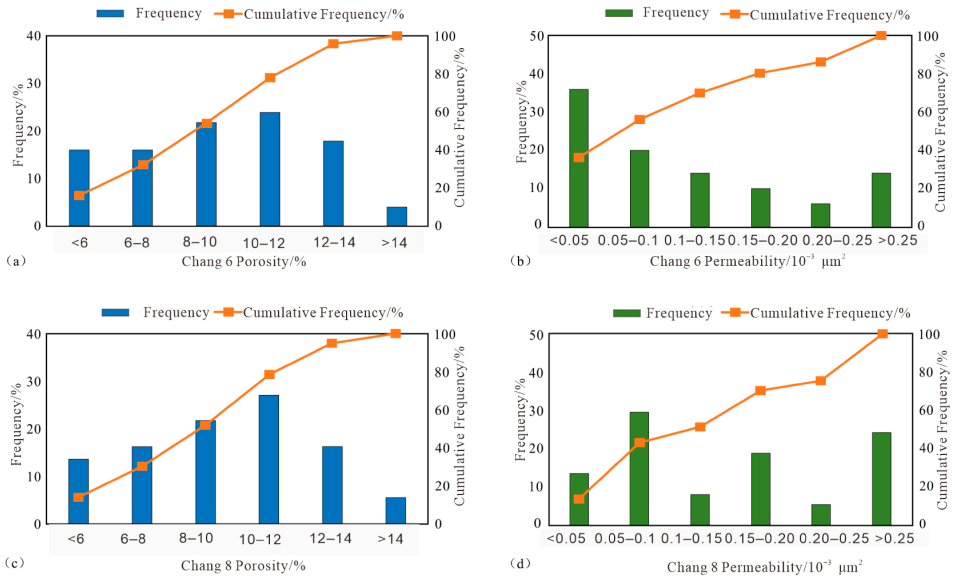


Figure 3. Distribution histogram of porosity and permeability of the Chang 6 and Chang 8 members. (**a**) Histogram and cumulative curve of porosity in the Chang 6 member. (**b**) Permeability histogram and cumulative curve of the Chang 6 member. (**c**) Histogram and cumulative curve of porosity in the Chang 8 member. (**d**) Permeability histogram and cumulative curve of the Chang 8 member.

First, porosity characteristics: The porosity histograms of Chang 6 (Figure 3a) and Chang 8 (Figure 3c) share nearly identical distribution schemes, with both intervals showing a frequency peak within the 10%–12% porosity bin, and consistent frequency proportions across all porosity grades from <6% to >14%. Statistical numerical results further verify this similarity: the Chang 6 member has a porosity ranging from 2.3%–15.5% (mean = 9.27% ± 0.7%), while the Chang 8 member has a porosity ranging from 5.1%–18.9% (mean = 9.88% ± 0.9%). The two sets of strata have similar average porosity values and similar overall porosity distributions.

Second, permeability distribution displays prominent differences between the two layers, as illustrated in Figure 3b,d. For the Chang 6 reservoir, the permeability frequency peak occurs at the $<0.05 \times 10^{-3}$ μm^2 bin; this interval accounts for an extraordinarily high proportion of samples, driving a steep rise in the cumulative frequency curve. This pattern demonstrates that Chang 6 is dominated by ultra-low permeability, corresponding to well-sorted, fine pore-throat assemblages. Its permeability ranges 0.006×10^{-3}–12.881×10^{-3} μm^2, with a geometric mean of 0.142×10^{-3} μm^2 and arithmetic mean of 0.38×10^{-3} μm^2.

By contrast, the Chang 8 reservoir exhibits a permeability frequency peak shifted toward the coarser 0.05–0.10×10^{-3} μm^2 bin, with samples broadly distributed across all permeability classes. The frequency variation between successive bins is modest, and the cumulative frequency curve rises gradually—a pattern indicative of poorer pore-throat sorting and a significantly higher proportion of relatively coarse throats relative to Chang 6. Quantitatively, Chang 8 permeability ranges from 0.023×10^{-3} to 18.65×10^{-3} μm^2, with geometric plus arithmetic means of 0.260×10^{-3} μm^2 and 0.89×10^{-3} μm^2, respectively—substantially exceeding the corresponding values for Chang 6.

Integration of the petrophysical frequency distributions and statistical parameters demonstrates that pore-throat architecture, as reflected by permeability, is the primary

control on fluid seepage capacity, eclipsing the role of total porosity. Although the two members share broadly comparable porosity distributions, their markedly contrasting permeability regimes and pore-throat configurations translate into a pronounced divergence in reservoir flow performance.

The porosity–permeability crossplot illustrates that permeability generally increases with rising porosity in both the Chang 6 and Chang 8 reservoirs, whereas the relatively scattered data reveals strong heterogeneity of pore structures in the study area (Figure 4). The two sets of reservoirs show wide overlapping ranges of porosity. Nevertheless, samples from the Chang 8 reservoir generally possess higher permeability at equivalent porosity values. The Chang 8 reservoir contains high-quality samples with a permeability greater than 1 mD and exhibits a much higher permeability upper limit, while such high-permeability samples are absent in the Chang 6 reservoir, which also has a higher proportion of extremely tight samples. These features indicate that porosity is not the exclusive factor controlling reservoir seepage capacity; pore-throat size and pore connectivity exert critical impacts. Compared with the Chang 6 reservoir, the Chang 8 reservoir is characterized by better pore connectivity and more developed effective pore throats with superior overall seepage performance, further demonstrating that the Chang 8 reservoir has better physical properties.

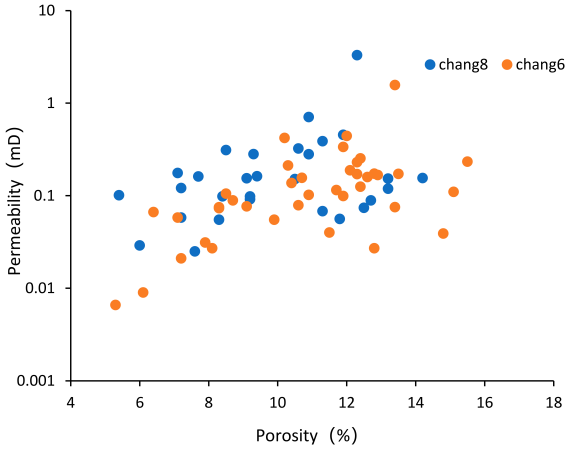


Figure 4. Porosity–permeability crossplot of Chang 6 and Chang 8 members.

In terms of reservoir classification, both the Chang 6 and Chang 8 members qualify as typical tight sandstones according to the criteria proposed by Sun et al. (2019) [1,2]. Comparison with global tight sandstone analogs reveals that the study-area reservoirs possess competitive physical properties. The Mesaverde Group (USA) exhibits 5%–12% porosity with permeability predominantly below 0.1×10^{-3} μm^2 [5,6]; offshore Jurassic tight gas sands in the Norwegian North Sea display 5%–15% porosity with a geometric mean permeability generally below 0.1×10^{-3} μm^2 [7]. Domestic analogs include the Penglaizhen Formation (Sichuan Basin: porosity 6%–12%, permeability mostly $< 0.3 \times 10^{-3}$ μm^2) and the Xujiahe Formation (porosity 7%–10%, permeability $< 0.2 \times 10^{-3}$ μm^2). The geometric mean permeability of the Chang 8 member (0.260×10^{-3} μm^2) falls within the upper tier of these global and regional tight sandstone benchmarks, underscoring its comparatively favorable flow capacity compared with comparable tight reservoirs.

4.3. Pore Types

Observation of epoxy-impregnated thin-section and SEM (Figure 5) shows that the pore types in the study area include intergranular pores, intergranular dissolution pores, feldspar dissolution pores, lithic dissolution pores, intercrystalline pores, and microfractures. Both members are dominated by intergranular pores and dissolution pores. The primary intergranular pore content (2.179%) and total plane porosity (3.270%) of the Chang

8 member are higher than those of the Chang 6 member (0.914% and 1.986%, respectively) (Table 2). Although microfractures account for only a small proportion, they are significant for improving reservoir connectivity.

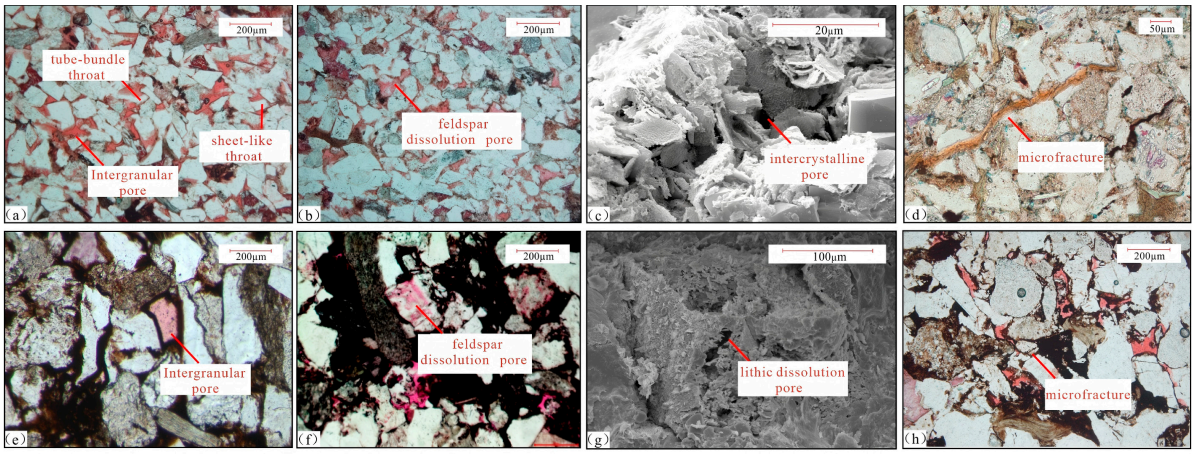


Figure 5. Pore-throat types of the Chang 6 and Chang 8 members in the Yuele Area, Ordos Basin. (**a**) Intergranular pore- and sheet-like and tubular throats, Well B280, 1892.44 m, Chang 6 member, cast thin section. (**b**) Intragranular dissolution pore in feldspar, Well B280, 1851.23 m, Chang 6 member, cast thin section. (**c**) Intercrystalline pore developed in kaolinite, Well Y436, 1971.24 m, Chang 6 member, SEM. (**d**) Microfracture, Well B143, 1927.5 m, Chang 6 member, cast thin section. (**e**) Intergranular pore, Well B280, 2214.84 m, Chang 8 member, cast thin section. (**f**) Feldspar dissolution pore, Well X315, 2085.8 m, Chang 8 member, cast thin section. (**g**) Lithic dissolution pore, Well W129, 2180.10 m, Chang 8 member, SEM. (**h**) Microfracture, Well B269, 2140.4 m, Chang 8 member, cast thin section.

Table 2. Reservoir space types of the Chang 6 member and Chang 8 member in the Yuele Area, Ordos Basin.

Member	Intergranular Pore (%)	Intergranular Dissolution Pore (%)	Feldspar Dissolution Pore (%)	Lithic Dissolution Pore (%)	Carbonate Dissolution Pore (%)	Matrix Dissolution Pore (%)	Intercrystalline Pore (%)	Microfracture (%)	Areal Porosity (%)
Chang 6	0.914	0.016	0.888	0.132	0.003	0.013	0.041	0.016	1.986
Chang 8	2.179	0.010	0.903	0.180	0.000	0.004	0.031	0.014	3.270

4.4. Microscopic Pore-Throat Characteristics

MIP measurements were performed to quantitatively characterize the pore-throat structure and classify the capillary pressure curve types of the Chang 6 and Chang 8 tight sandstone reservoirs (Table 3; Figure 6). Four typical mercury intrusion curve patterns (Type I, II, III, and IV) with distinct morphological features and parametric thresholds were identified for the two reservoir intervals, showing significant sedimentary–diagenetic heterogeneity between turbidite and delta-front sandstones.

For the Chang 8 delta-front tight sandstones, Type I curves present an obvious flat plateau shape, characterized by low displacement pressure (<0.5 MPa), large median throat radius (>0.2 μm), high mercury ejection efficiency (>35%), a porosity greater than 12%, and permeability exceeding 0.6 × 10 μm, indicative of a coarse skewed distribution and excellent pore-throat connectivity. Type II curves display a slightly sloped plateau with moderate displacement pressure (0.5–1.0 MPa), a median throat radius over 0.18 μm, mercury ejection efficiency higher than 32%, porosity of 10%–12%, and permeability ranging from 0.2 × 10 to 0.6 × 10 μm, representing a moderately favorable pore structure. Type III curves exhibit a steepened plateau with medium–high displacement pressure (1.0–2.0 MPa), a small median throat radius (0.01–0.18 μm), a mercury ejection efficiency above 25%, porosity of 6%–10%, and a permeability of 0.05 × 10–0.2 × 10 μm, corresponding to poor pore-throat sorting.

Type IV curves show an extremely steep slope without obvious plateau features, with high displacement pressure (>2.0 MPa), a tiny median throat radius (<0.1 μm), low mercury ejection efficiency (<25%), a porosity below 8%, and a permeability of less than 0.1 × 10 μm, representing the poorest reservoir pore structure (Figure 6b).

Table 3. Statistical table of mercury injection parameters of Chang 6 and Chang 8 members in the Yuele Area, Ordos Basin.

Member	Type	Porosity (%)	Permeability (mD)	Displacement Pressure (MPa)	Median Radius (μm)	Median Pressure (MPa)	Sorting Coeffi-cient	Coefficient of Variation	Skewness	Max SHg (%)	Mercury Ejection Efficiency (%)
Chang 6	Minimum Value	5.30	0.007	0.060	0.020	1.126	0.573	0.041	−1.562	57.99	9.90
	Maximum Value	15.50	1.568	16.034	0.653	36.346	2.546	0.229	1.724	96.17	37.30
	Mean Value	10.80	0.196	3.564	0.128	11.189	1.399	0.115	0.024	77.49	25.05
Chang 8	Minimum Value	5.10	0.023	0.215	0.018	1.204	0.834	0.062	−1.164	53.20	10.19
	Maximum Value	13.20	3.300	24.276	0.611	40.314	3.003	0.291	1.915	92.49	40.00
	Mean Value	9.70	0.298	3.875	0.137	12.455	1.882	0.165	0.446	77.88	27.49

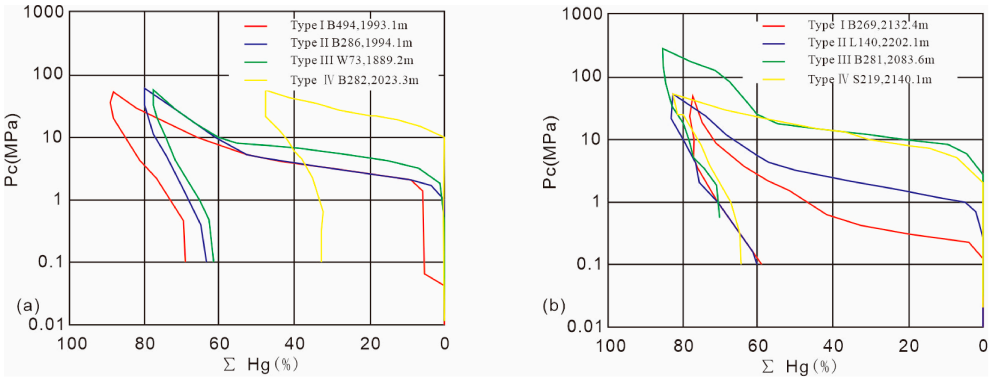


Figure 6. Characteristics and classification of mercury intrusion curves for Chang 6 and Chang 8 reservoirs. (**a**) mercury intrusion curves of the Chang 6 reservoir; (**b**) mercury intrusion curves of the Chang 8 reservoir.

In comparison, Chang 6 turbidite tight sandstones exhibit an overall inferior pore structure with stricter parametric thresholds for each curve type. Chang 6 Type I curves show a flat plateau and good pore connectivity, but require a higher displacement pressure (<1.0 MPa), lower median throat radius (>0.15 μm), and lower mercury ejection efficiency (>23.0%), with porosity > 11% and permeability > 0.12 × 10 μm. Chang 6 Type II curves are morphologically similar to Type I but with a moderate displacement pressure of 1.0–2.0 MPa, median throat radius of 0.10–0.16 μm, mercury ejection efficiency of 20%–30%, porosity of 8.5%–13.5%, and permeability of 0.10 × 10–0.20 × 10 μm. Chang 6 Type III curves possess a steep plateau and high displacement pressure (2.0–4.0 MPa), with a median throat radius of 0.035–0.16 μm, mercury ejection efficiency of 17.89%–37.74%, porosity of 7.1%–12.0%, and permeability of 0.08 × 10–0.20 × 10 μm. Chang 6 Type IV curves are dominated by steep-slope patterns with extremely high displacement pressure (>4.0 MPa), median throat radius generally less than 0.1 μm, mercury ejection efficiency lower than 29%, porosity below 8%, and permeability of less than 0.1 × 10 μm, indicating severely poor pore-throat physical properties (Figure 6a).

MIP statistical results (Table 3) further verify the above curve-based heterogeneity. For the Chang 6 member, the average median throat radius is 0.128 μm (dominated by

fine pore throats), with a sorting coefficient of 1.399, skewness of 0.024 (coarse skewed), mercury ejection efficiency of 25.05%, and displacement pressure of 3.56 MPa. For the Chang 8 member, the average median throat radius reaches 0.137 μm (dominated by medium-fine pore throats), with a sorting coefficient of 1.882, skewness of 0.446 (coarse skewed), mercury ejection efficiency of 27.49%, and displacement pressure of 3.88 MPa. The homogeneity coefficient is slightly lower for the Chang 8 member, suggesting that larger throats in Chang 8 contribute more effectively to permeability [22]. Combined with curve morphological differences, the Chang 8 delta-front sandstones develop more high-quality Type I and II pore structures with coarser pore throats, better connectivity and higher mercury ejection efficiency, while Chang 6 turbidites are dominated by Type III and IV poor pore structures with finer throats, higher displacement pressure and weaker pore connectivity. In summary, the overall pore-throat structure and reservoir physical performance of the Chang 8 member are significantly superior to those of the Chang 6 member.

The median pore-throat radii of samples from the Chang 6 and Chang 8 reservoirs largely overlap, and mainly range from 0 to 0.25 μm (Figure 7). Nevertheless, significant differences exist in their pore-throat structure characteristics. The maximum median pore-throat radius of the Chang 6 reservoir is approximately 0.30 μm, and samples with large pore throats are absent. A considerable number of samples exhibit a displacement pressure higher than 5 MPa, indicating a high proportion of tight reservoirs. In contrast, the Chang 8 reservoir possesses a wider distribution range of pore throats, with multiple samples representing favorable reservoirs characterized by a median pore-throat radius greater than 0.3 μm and low displacement pressure. Affected by reservoir heterogeneity, the displacement pressure shows obvious dispersion at equivalent median pore-throat radius. This can be attributed to the fact that displacement pressure is controlled by the maximum connected pore throat, whereas the median pore-throat radius only reflects the overall level of pore throats. Furthermore, variations in pore-throat sorting, connectivity and mineral composition further increase the parameter dispersion. Overall, the Chang 8 reservoir is favorable for the development of high-quality reservoirs with larger pore throats, and its development degree of favorable reservoirs is superior to that of the Chang 6 reservoir.

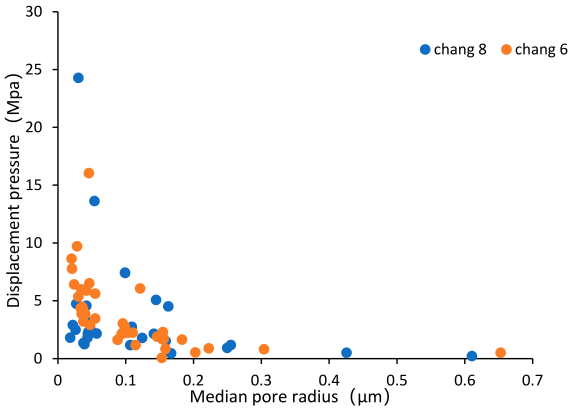


Figure 7. Crossplot of displacement pressure versus median pore-throat radius for the Chang 6 and Chang 8 reservoirs.

5. Discussion

5.1. Coupled Sedimentary–Diagenetic Evolution and Reservoir Quality Differentiation

Reservoir physical properties result from the coupling of sedimentation (Figure 8) and diagenesis [8,20]. Sedimentation lays the foundation for primary pores, while diagenesis profoundly modifies them. Using the method of Beard and Weyl (1973), we estimated original porosity (Φ_0) for an idealized well-sorted sand as ~47% (46.60% for Chang 6, 47.48%

for Chang 8) [20]. Based on point-count data and the approach of Houseknecht (1987), we partitioned total porosity loss (Φ_0 − measured Φ) into compaction loss (reduction in intergranular volume not filled by cement) and cementation/dissolution loss (volume of cements ± secondary porosity) [19]. This approach suggests that compaction accounts for approximately 50%–55% of total porosity loss, and diagenetic mechanisms (cementation ± dissolution) account for 45%–50%. Sedimentation establishes the material basis for reservoir pore development, whereas diagenesis dominates the post-burial modification of primary pores. These two geological mechanisms, together, govern reservoir quality from a genetic perspective; however, constrained by differences in clastic composition and burial conditions, their actual contributions to reservoir physical properties vary across strata.

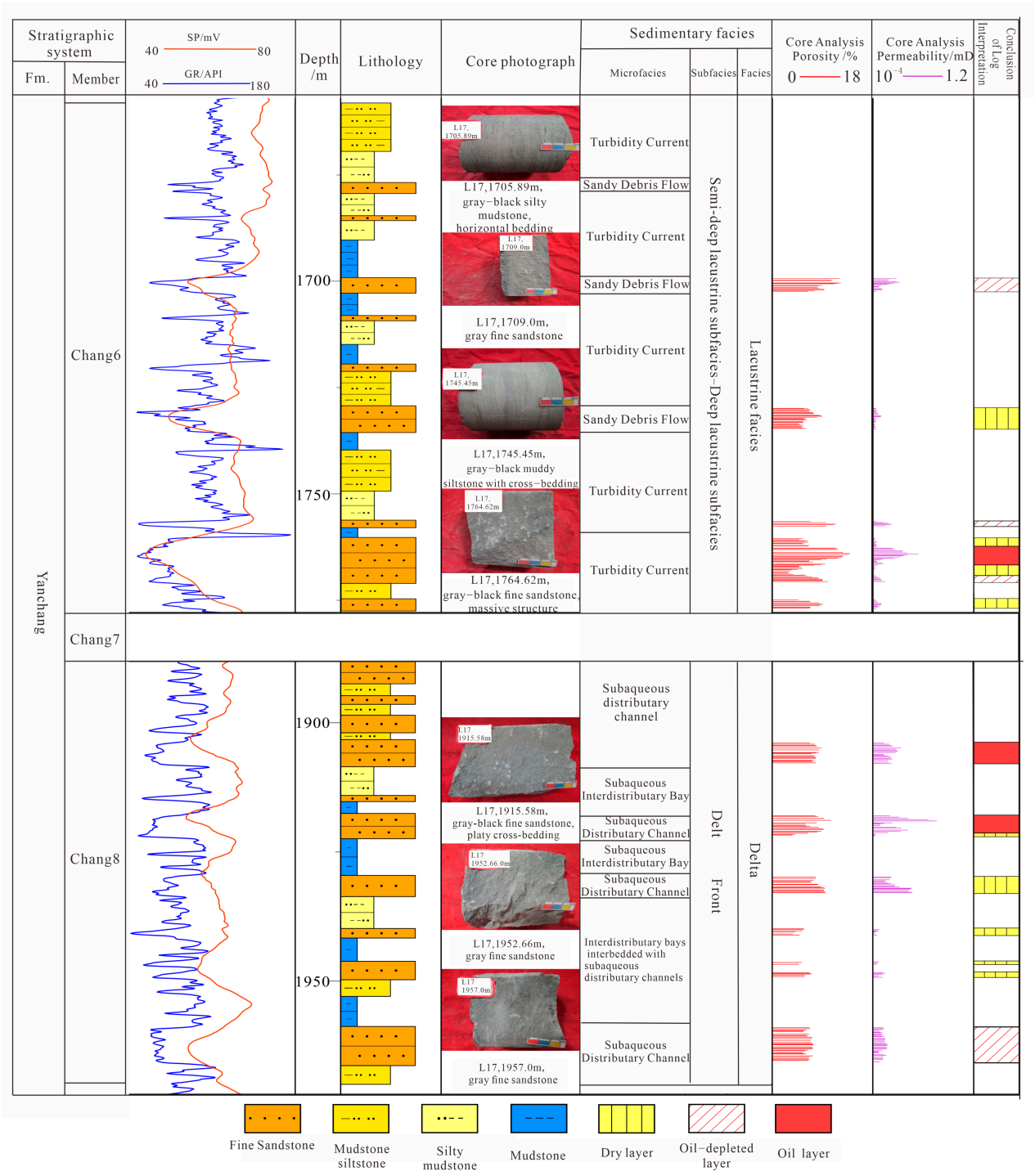


Figure 8. Deposition–lithology–physical relationship between the Chang 6 member and Chang 8 member.

Within this analytical framework, two distinct sedimentary–diagenetic pore evolution pathways are reconstructed (Figure 6). All pore evolution calculations rely on the empirical porosity model from Beard and Weyl (1973) [20], which takes the ideal primary porosity of well-sorted sandstones as the baseline. Adopting the quantitative decomposition scheme refined by Xu (2024) [23], total porosity change is divided into three components: compaction-induced porosity reduction, cementation-related porosity loss, and dissolution-generated secondary porosity. The evolutionary pathway of Chang 8 (high-quality reservoir) is detailed below (Figure 9).

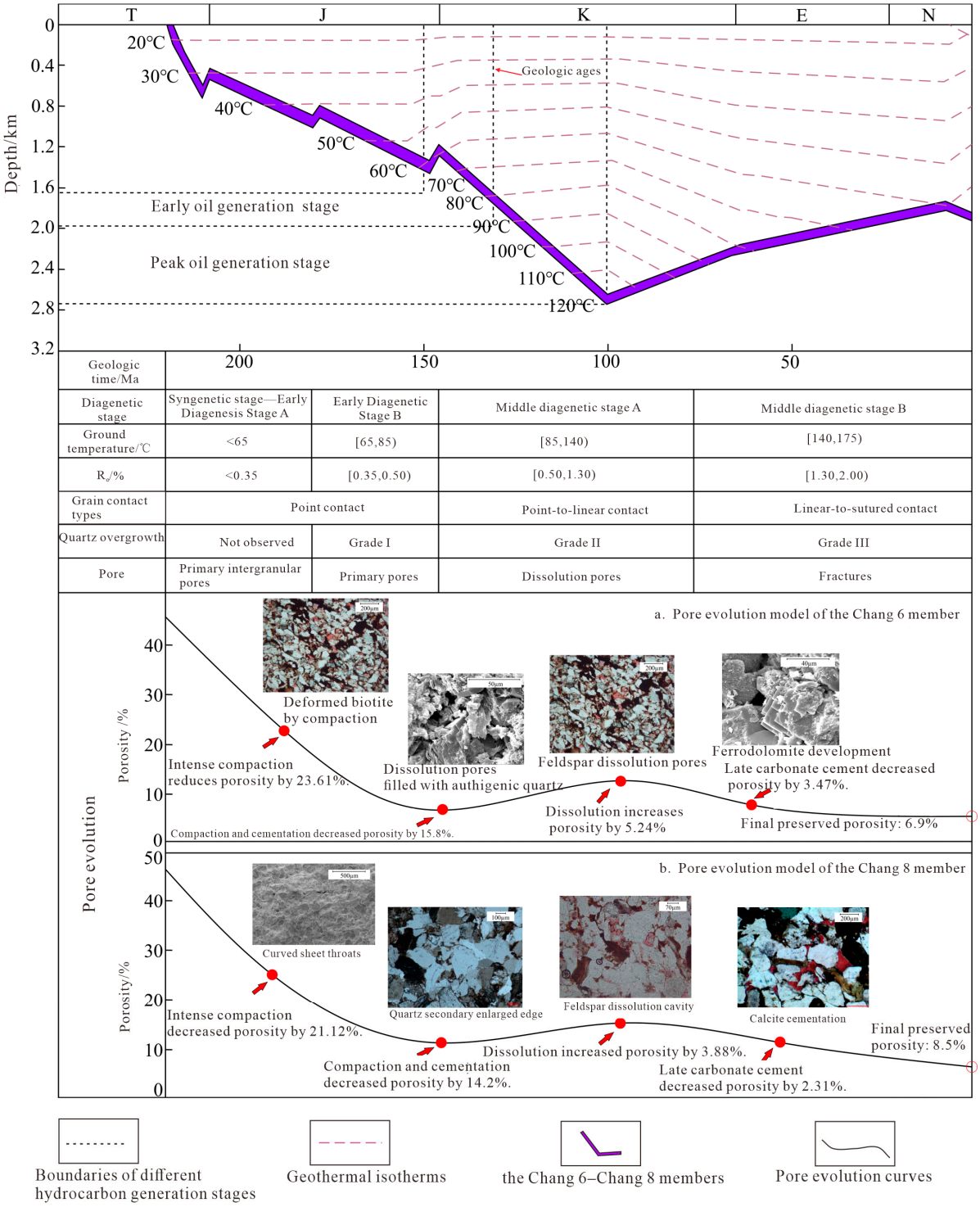


Figure 9. Comparison of pore evolution history between the Chang 6 member and the Chang 8 member in the Yuele area, Ordos Basin.

This route begins with delta-front deposits characterized by elevated textural maturity—i.e., coarser grain sizes (0.15–0.5 mm), good roundness, well sorting (Figure 10), and minimal mud admixture—coupled with an abundance of magmatic lithic fragments (7.08%) (Table 4). During early diagenesis, alterations in these Fe- and Mg-rich volcanic components generate pore-lining chlorite coats (averaging 5.13%) (Figure 11). Chlorite films then: (i) mechanically strengthen framework grains, enhancing compaction resistance; (ii) inhibit quartz overgrowth, preserving primary pores; and (iii) provide pathways for later dissolution by acidic fluids. Consequently, despite the greater burial depth, porosity loss from compaction is lower (21.12% vs. 23.61% for Chang 6), and a larger proportion of primary intergranular pores (2.179%) is preserved, forming a composite pore network with favorable pore-throat connectivity (Figure 11).

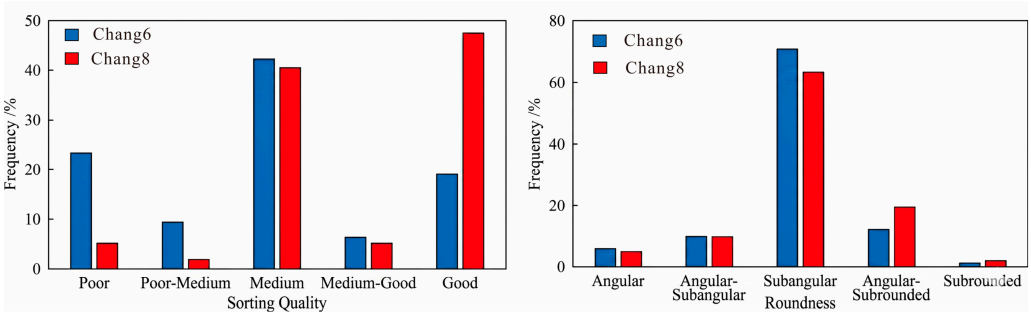


Figure 10. Histogram of sorting and roundness distribution of the Chang 6 and Chang 8 members in the Yuele Area, Ordos Basin.

Table 4. Types of interstitials of the Chang 6 and 8 member sandstone in the Yuele Area, Ordos Basin.

Member	Type	Main Interstitial Materials (%)						
		Kaolinite	Illite	Chlorite	Calcite	Ferrocalcite	Ankerite	Siliceous
Chang 6	Maximum Value	7.00	44.00	25.70	19.80	37.80	34.20	6.40
	Mean Value	0.04	7.31	2.48	0.32	2.31	0.84	1.35
Chang 8	Maximum Value	6.40	21.80	18.20	6.00	18.20	2.00	7.20
	Mean Value	0.16	2.78	5.13	0.26	1.86	0.19	1.78

The above diagenetic sequence enables Chang 8 sandstones to retain abundant primary intergranular pores and favorable pore-throat connectivity. In sharp contrast, the turbidite Chang 6 member lacks protective chlorite coatings and undergoes a completely different pore-evolution process dominated by severe pore occlusion, as outlined in the evolutionary course for Chang 6 (poorer quality reservoir) (Figure 9).

This alternative trajectory involves semi-deep to deep lacustrine turbidites that exhibit low textural maturity (fine grain sizes of 0.05–0.3 mm, poor roundness, poor sorting, appreciable clay content) and a scarcity of magmatic rock fragments (only 2.53%). In the absence of protective chlorite coats, mechanical compaction proceeds vigorously, causing ductile grains (micas, phyllite clasts) to deform and intrude into adjacent pore spaces (Figure 12). Subsequently, potassium-rich fluids induce the precipitation of abundant hairy illite (7.31%), which divides large pores and blocks throats. Combined with carbonate cement filling (3.47%), this forms an isolated pore system dominated by micropores and intercrystalline pores, resulting in extremely low permeability.

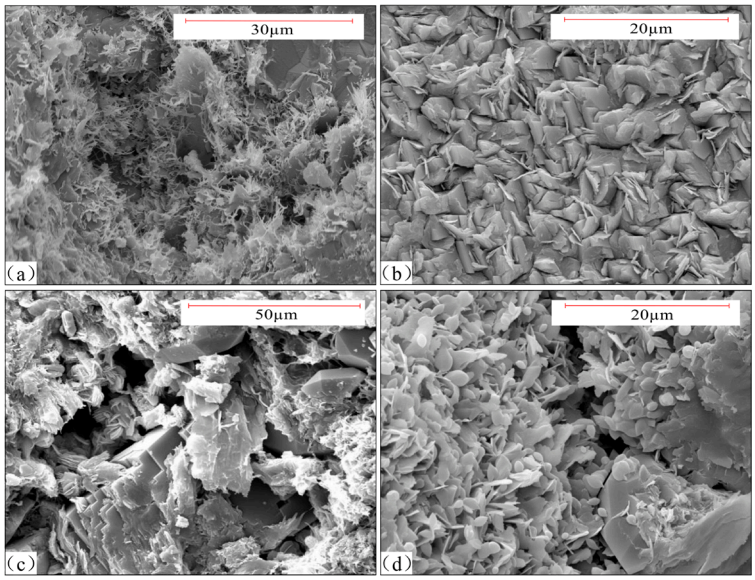


Figure 11. Development characteristics of illite and chlorite in tight reservoirs of the Chang 6 and Chang 8 members in the Yuele area, Ordos Basin. (**a**) Hair-like illite aggregates filling intergranular pores, Well Z74, 1599.93 m, Chang 6 member; (**b**) Scaly illite, Well S209, 2194.50 m, Chang 8 member; (**c**) Leaf-like chlorite filling intergranular pores, Well S159, 2100.15 m, Chang 6 member; (**d**) Centripetally grown pore-lining chlorite coats, narrowing intergranular pores and forming pore throats, Well S184, 2214.60 m, Chang 8 member.

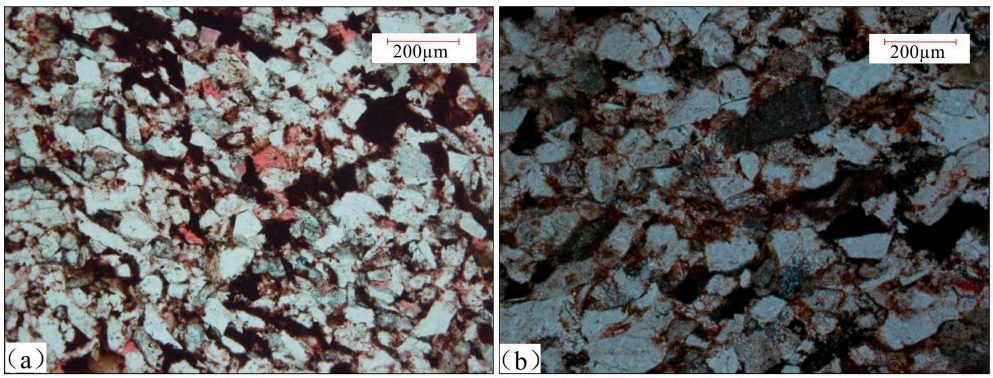


Figure 12. Compaction characteristics of Chang 6 and Chang 8 tight reservoirs in the Yuele Area, Ordos Basin. (**a**) Compressive bending deformation of biotite, Well B281, 1979.2 m, Chang 6 member; (**b**) Igneous rock debris, Well L181, 2099.06 m, Chang 8 member.

Three interrelated K^+ supply mechanisms jointly account for the abundant fibrous illite within Chang 6 turbidites, modulated by prolonged source-to-sink transport and turbidite-specific lithology [24–26]. First, intense mechanical compaction promotes the pressure dissolution of detrital muscovite, biotite and K-feldspar. Unlike Chang 8 delta-front sandstones, which are protected by continuous grain-coating chlorite, Chang 6 lacks rigid chlorite frameworks to support grains, accelerating silicate decomposition and continuous K^+ release into pore water [12,24]. Second, the thick muddy matrix delivered via long-distance turbidity transport is rich in detrital smectite. Within burial temperature windows of 90–130 °C, progressive smectite-to-illite transformation consumes pore-water K^+ and generates fibrous pore-filling illite; this clay conversion cycle continuously elevates fluid potassium activity [25,27]. Third, long source-to-sink transport fundamentally shapes the above two K-providing processes. During far-field turbidity transport, labile magmatic fragments are fully weathered and depleted, eliminating early chlorite formation; meanwhile, fine-grained muddy detritus and K-bearing sheet silicates accumulate massively in

semi-deep lacustrine turbidite bodies, establishing a favorable material basis for later K^+ enrichment and illitization.

Overall, the distinct source-to-sink transport distance between Chang 6 and Chang 8 drives lithological discrepancies, which further control the intensity of silicate pressure solution and clay mineral transformation, forming a complete genetic chain linking sedimentary routing, K^+ fluid evolution and illite–cement-induced reservoir deterioration [12,26].

The evolutionary courses documented here are comparable to those observed in other tight sandstone basins [5–7]. In the Mesaverde Group (USA), reservoir quality is strongly influenced by authigenic clays: chlorite preserves porosity by inhibiting quartz cement, while illite severely reduces permeability [5,6]. Similarly, in the Norwegian North Sea tight gas sands, early chlorite coatings are critical for preserving porosity at depths > 4 km, whereas illite-rich sandstones show severely degraded permeability despite moderate porosity [7]. Our findings thus reinforce a general principle: the presence or absence of early chlorite films is a key threshold control on diagenetic differentiation in tight sandstones throughout diverse sedimentary basins [9,28–30].

Two prerequisites are required for chlorite film development: (i) sufficient supply of Fe- and Mg-rich volcanic materials during sedimentation; (ii) relatively strong hydrodynamic conditions providing low mud content and adequate space for fluid migration and chlorite precipitation.

5.2. Comparison with Regional Framework and Local Provenance Effects

The regional diagenetic model proposed by Liu et al. (2018) [12] for the Longdong area highlights three key controls: pore-throat characteristics govern physical properties; chlorite cement preserves porosity; and illite, together with carbonate cements, reduces permeability. Our independent dataset from the Yuele Area confirms this system across all three aspects.

Within this established context, the abundant core samples collected in this work allow for a quantitative comparison of local mineral parameters against the Longdong regional baseline (Table 5). The Yuele Area lies closer to the basin's southwestern sediment source. As a result, its Chang 8 member contains more magmatic rock fragments (7.08%) and consequently more chlorite (5.13%) than the Longdong regional standards (roughly 4%–5% magmatic debris and 3.5%–4.0% chlorite). This proximity to provenance increases the pore-preserving effect. However, the Chang 6 member in Yuele exhibits elevated illite content (7.31% versus the regional range of 5%–6%), suggesting more intense illite cementation—likely linked to greater water depth during deposition, higher background mud content, and potassium ion enrichment in diagenetic fluids. These observations emphasize that even within a single basin, reservoir quality can vary considerably across sub-basinal structural units, necessitating local, zone-by-zone evaluation.

A comparative analysis of our measurements and the Longdong diagenetic model yields two novel insights that distinguish this work from previous regional studies. Most existing comparative investigations of the Chang 6 and Chang 8 members provide only qualitative descriptions of sedimentary environments and a simple collation of bulk mineral and petrophysical data, without establishing quantitative linkages among provenance supply, clastic assemblages, authigenic clay minerals, and microscale pore-throat geometry. Supported by multi-scale core and microscopic observations, this study reconstructs a complete evolutionary chain spanning sediment source, post-depositional diagenetic modification and final reservoir quality—an analytical approach rarely adopted in previous basin-wide comparative work.

Furthermore, the original Longdong diagenetic summary was established using samples from districts far from the southwestern provenance and remains purely qualitative,

which risks biased reservoir evaluation when applied to proximal blocks. By quantitatively characterizing how magmatic lithic, chlorite and illite contents shift with provenance distance, this paper establishes facies-specific discriminant criteria for high-quality reservoirs. These mineralogical proxies can be applied to core-based reservoir grading and well placement optimization, delivering practical value for field exploration.

Table 5. Comparison of key parameters between the Yuele Area and Longdong Area (Liu Hanlin et al., 2018) [12].

Comparison Items	Yuele Region (This Study)	Longdong Region (Liu Hanlin et al., 2018)	Contrastive Meaning
Content of chlorite in Chang 8 member	5.13%	Approximately 3.5%–4.0% (regional average)	Yuele area is higher than the regional average, reflecting local differences in material sources
Content of magmatic rock debris in Chang 8 member	7.08%	Approximately 4%–5% (regional average)	Confirming source differences: Yuele area is closer to the southwest source area
Illite content in Chang 6 member	7.31%	Approximately 5%–6% (regional average)	Yuele area is higher than the regional average, with stronger diagenetic damage
Compaction porosity reduction rate of Chang 8 member	21.12%	Approximately 15% (regional average)	The calculation caliber is consistent, reflecting the same compaction trend
Compaction porosity reduction rate of Chang 6 member	23.61%	Approximately 17% (regional average)	The calculation caliber is consistent, reflecting the same compaction trend
Permeability ratio between Chang 8 member and Chang 6 member	Chang 8/Chang 6 $\approx$ 1.83	Chang 8/Chang 6 $\approx$ 1.5%–2.0	Highly consistent with regional patterns

Collectively, this research addresses the common drawback of evaluating tight sandstones solely on the basis of single porosity–permeability indices or undifferentiated interformational comparisons. Integrated quantitative coupling between sedimentary and diagenetic processes verifies that authigenic clay mineral differentiation acts as a critical threshold factor driving the permeability contrast between the two sandstone types. The quantified provenance-controlled mineral variation patterns supplemented herein also provide a replicable analytical workflow for comparative research on analogous lacustrine tight sandstone systems worldwide.

5.3. Consequences for Tight Sandstone Exploration

Based on the comparative study presented above, we propose the following guidelines for tight sandstone exploration in the southwestern Ordos Basin and analogous lacustrine basins.

High quartz content is not a reliable proxy for reservoir quality. Although the Chang 6 member has a higher quartz fraction (33.96%), its reservoir performance is poor because it lacks chlorite protection and is severely illite-cemented (Figure 13). Evaluation efforts ought to prioritize diagenetic pathways, especially the early formation of chlorite films.

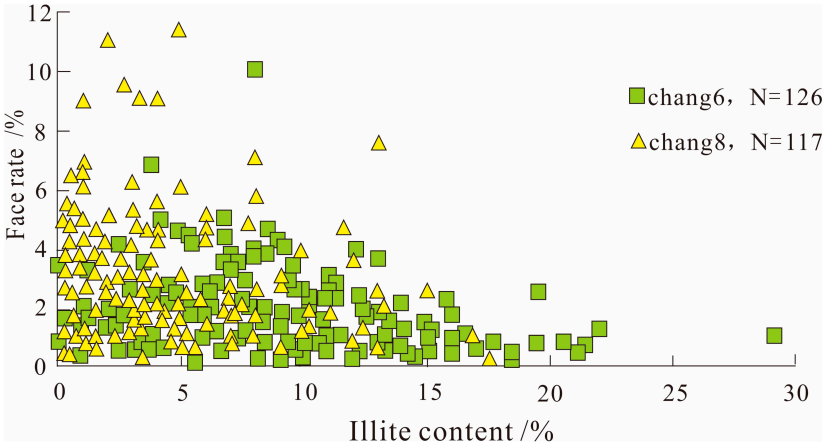


Figure 13. Correlation between reservoir facies and illite volume fraction of the Chang 6 and Chang 8 members in the Yuele area, Ordos Basin.

There is no simple linear correlation between areal chlorite content and areal porosity (Figure 14). Samples with chlorite areal content ranging from 3% to 10% tend to exhibit relatively high areal porosity, while most samples show decreased porosity when chlorite content exceeds 10%. This feature is jointly controlled by chlorite occurrence. Continuous grain-coating chlorite (content > 3%) can inhibit quartz overgrowth and preserve primary pores. Nevertheless, a further increase in total chlorite content (>10%) implies a higher proportion of pore-filling chlorite, which occupies pore space and reduces areal porosity. Comparatively, numerous Chang 8 samples with high areal porosity occur within the 3%–10% chlorite interval, whereas such favorable samples are rare in the Chang 6 reservoir.

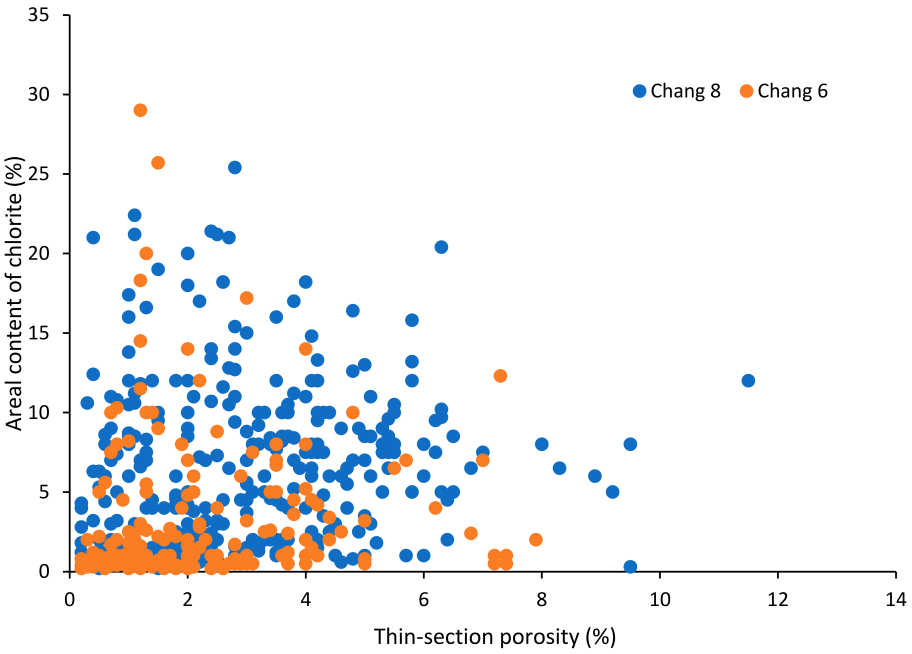


Figure 14. Crossplot of thin-section porosity versus areal content of chlorite.

Differences in chlorite enrichment display obvious spatial heterogeneity across the study area. Within the Longdong area, blocks nearer to the southwestern provenance—such as Yuele—display higher chlorite and better reservoir properties. Developing log-based predictive approaches for chlorite abundance could help identify sweet-spot intervals in uncored wells.

Delta-front deposits represent the most favorable facies belt. The distributary channel sand bodies of the Chang 8 member within the delta front combine high textural maturity with a favorable diagenetic evolution path, making them primary targets for finding relatively high-permeability reservoirs. In contrast, turbidite sand bodies in semi-deep to deep lacustrine settings undergo severe diagenetic degradation. Even when they retain moderate porosity, these materials' permeability remains extremely low; therefore, their economic recoverability should be assessed with caution.

5.4. Limitations and Future Directions

Several limitations of this study should be acknowledged. First, core sampling is limited to a few wells and may miss finer-scale lateral heterogeneities. Second, the analytical methods employed—thin-section petrography and MIP in particular—have finite resolution and may not completely resolve the full complexity of pore-throat networks, especially features at the nanometer scale. Third, the quantitative partitioning of porosity loss between compaction and cementation relies on an assumed initial porosity value for well-sorted sands (Beard and Weyl, 1973) and therefore has inherent uncertainty; the results are best interpreted as relative trends rather than absolute values [20].

Upcoming investigations would benefit from: (a) higher-density sampling in underexplored intervals and areas close to provenance; (b) the application of advanced techniques such as automated mineralogy and three-dimensional pore-network reconstruction (e.g., micro-CT); (c) the development of multi-parameter anticipatory models which integrate petrological, diagenetic, and sedimentological data; and (d) geochemical and isotopic approaches (including stable isotopes and fluid inclusion analysis) to better constrain the timing of diagenetic events, thereby permitting more accurate reconstruction of reservoir evolution histories. Such efforts will improve sweet-spot prediction not only in the Ordos Basin but also in analogous tight sandstone systems internationally.

6. Conclusions

Based on petrographic, SEM, MIP and core physical tests, this study contrasts reservoir heterogeneity of Chang 6 turbidite and Chang 8 delta-front tight sandstones in the Yuele Block, Ordos Basin. Core conclusions are summarized below:

1. Lacustrine tight sandstones feature obvious porosity–permeability decoupling, which revises reservoir evaluation criteria. Though Chang 6 and Chang 8 have similar bulk porosity, their fluid deliverability varies sharply. Burial diagenesis reshapes pore-throat geometry and connectivity, the dominant controls on reservoir quality; microscale pore-throat architecture is therefore the primary grading metric for tight sand reservoirs.
2. Source-to-sink transport distance, which is differentiated intrinsically by sedimentary facies, dominates diagenetic divergence (core innovation). Short transport paths in Chang 8 proximal delta-front sandstones deliver abundant magmatic clastics, forming pervasive early grain-coating chlorite that suppresses compaction and quartz overgrowth to retain primary pores. By contrast, Chang 6 semi-deep lacustrine turbidites experience long-distance transport with scarce magmatic debris and lack chlorite protection; severe compaction followed by massive illite–carbonate cementation blocks pore throats and generates isolated low-permeability micropores. This work establishes a quantitative coupling chain of "provenance supply—authigenic clay evolution—pore evolution". Consistent burial–thermal histories between Yuele and Longdong verify that shorter transport distances boost magmatic lithic and chlorite contents in delta-front sands, while longer transport aggravates illite cementation

in turbidites. Such mineral indicators complement regional diagenetic models and enhance sweet-spot prediction for near-source tight oil reservoirs.

3. This study has two main limitations: the uneven core distribution and limited resolution of conventional methods fail to fully characterize lateral micro-heterogeneity and nanoscale pore evolution. Future work can adopt Micro-CT 3D pore reconstruction and fluid inclusion geochemistry to constrain chlorite formation timing and reconstruct multi-stage water—rock interactions, perfecting diagenetic evolution theories for continental lacustrine tight sandstones.

Author Contributions: C.L. (Chi Li): Conceptualization, Formal analysis, Investigation, Writing—original draft. C.L. (Cheng Li) and X.Z.: Writing—review. Y.B.: Editing. L.X. and Q.P.: Drawing. Q.W.: Conceptualization, Writing—review and editing. All authors have read and agreed to the published version of the manuscript.

Funding: This research received no external funding.

Data Availability Statement: The datasets presented in this article are not readily available due to commercial confidentiality restrictions. Requests to access the datasets should be directed to the corresponding author once the commercial restrictions are lifted.

Conflicts of Interest: Chi Li, Cheng Li, Yujie Bai and Xiaohui Zhang are employees of PetroChina Changqing Oilfield Company The paper reflects the views of the scientists and not the company.

References

1. Sun, L.; Zou, C.; Jia, A.; Wei, Y.; Zhu, R.; Wu, S.; Guo, Z. Development characteristics and orientation of tight oil and gas in China. *Pet. Explor. Dev.* **2019**, *46*, 1015–1026. [CrossRef]
2. Li, G.; Zhu, R. Progress, challenges and key issues of unconventional oil and gas development of CNPC. *China Pet. Explor.* **2020**, *25*, 1–13.
3. Yang, H.; Li, S.; Liu, X. Characteristics and resource prospects of tight oil and shale oil in Ordos Basin. *Acta Pet. Sin.* **2013**, *34*, 1–11.
4. Yang, Z.; Fu, J.; Guo, Q.; Lin, S.; Chen, N.; Pan, S.; Li, S. Discovery, characteristics and resource potential of continental tight oil in Triassic Yanchang Formation, Ordos Basin. *China Pet. Explor.* **2017**, *22*, 9–15.
5. Stroker, T.M.; Harris, N.B.; Elliott, W.C.; Wampler, J.M. Diagenesis of a tight gas sand reservoir: Upper Cretaceous Mesaverde Group, Piceance Basin, Colorado. *Mar. Pet. Geol.* **2013**, *40*, 48–68. [CrossRef]
6. Spencer, C.W. Geologic Aspects of Tight Gas Reservoirs in the Rocky Mountain Region. *J. Pet. Technol.* **1983**, *37*, 1308–1314.
7. Ramm, M. Porosity-depth trends in reservoir sandstones: Theoretical models related to Jurassic sandstones offshore Norway. *Mar. Pet. Geol.* **1992**, *9*, 553–567. [CrossRef]
8. Morad, S.; Al-Ramadan, K.; Ketzer, J.M.; De Ros, L.F. The impact of diagenesis on the heterogeneity of sandstone reservoirs: A review of the role of depositional facies and sequence stratigraphy. *AAPG Bull.* **2010**, *94*, 1267–1309. [CrossRef]
9. Ehrenberg, S.N. Relationship between diagenesis and reservoir quality in sandstones of the garn formation, haltenbanken, mid-norwegian continental shelf. *AAPG Bull.* **1990**, *74*, 1538–1558. [CrossRef]
10. Xiao, L.; Wei, Q.; Lv, Y. The reservoir densification and the main controlling factors of high quality reservoir of Chang 6 reservoir in Nanliang area, Ordos Basin. *J. Yan'an Univ. (Nat. Sci. Ed.)* **2017**, *36*, 12–16.
11. Zhang, H.; Wei, Q.; Chen, X.; Bi, L.; Wei, X. Analysis of reservoir characteristics and main controlling factors of Chang 6 member in Yuele area, Ordos Basin. *J. Chengdu Univ. Technol.* **2024**, *51*, 531–542.
12. Liu, H.; Yang, Y.; Wang, F.; Deng, X.; Liu, Y.; Nan, J.; Wang, J.; Zhang, H. Micro pore and throat characteristics and origin of tight sandstone reservoirs: A case study of the Triassic Chang 6 and Chang 8 members in Longdong area, Ordos Basin, NW China. *Pet. Explor. Dev.* **2018**, *45*, 223–234. [CrossRef]
13. Zhong, H.; Wang, G.; Wu, J.; Cai, Y.; Li, H.; Liu, M. Influence of differential diagenesis of Chang 8 tight sandstone reservoirs in Qingcheng area on oil bearing properties. *Pet. Geol. Recovery Effic.* **2025**, *32*, 82–93.
14. Deng, X.; Ling, F.; Liu, X.; Pang, J.; Lv, J.; Li, S.; Liu, X. Discussion on relationship between sedimentary evolution of the Triassic Yanchang Formation and the Early Indosinian Movement in Ordos Basin. *J. Palaeogeogr. (Chin. Ed.)* **2008**, *2*, 159–166.
15. Wang, C.; Wei, Q.; Hu, R.; Xiao, L. Microstructure characteristics and genetic analysis of tight reservoirs with different provenance systems: A case study of Fanjiachuan and Nanliang region of Chang 6 reservoir in Longdong area, Ordos Basin. *Bull. Geol. Sci. Technol.* **2023**, *42*, 286–298.
16. Yang, J. *Tectonic Evolution and Hydrocarbon Distribution in Ordos Basin*; Petroleum Industry Press: Beijing, China, 2002.

17. Zhang, Y.; Ren, Z.; He, F.; Cui, J.; Yang, G.; Wang, K.; Ji, Y. Meso-Cenozoic structural characteristics and their reservoir controls of structural transition area in China Craton: A case study of Yanchang Formation in Zhenjing area of southwestern Ordos Basin. *Acta Petrol. Sin.* **2020**, *36*, 3537–3549. [CrossRef]
18. *SY/T 5336-2006*; Practices for Core Analysis. National Development and Reform Commission (NDRC): Beijing, China, 2006.
19. Houseknecht, D.W. Assessing the relative importance of compaction processes and cementation to reduction of porosity in sandstones. *AAPG Bull.* **1987**, *71*, 633–644. [CrossRef]
20. Beard, D.C.; Weyl, P.K. Influence of Texture on Porosity and Permeability of Unconsolidated Sand. *AAPG Bull.* **1973**, *57*, 349–369. [CrossRef]
21. Folk, R.L. *Petrology of Sedimentary Rocks*; Hemphill's Book Store: Austin, TX, USA, 1968.
22. Gao, H.; Sun, W. Quantitative evaluation method of microscopic pore-throat heterogeneity for low-permeability clastic reservoirs. *Geol. Sci. Technol. Bull.* **2010**, *29*, 78–83.
23. Xu, G.J.; Li, H.; Tang, L.; Gong, X.k.; Xie, Y.X.; Zhao, D.N.; Chen, J.m.; Wei, Q.L. Influence of pore structure characteristics on the Permian Shan-1 reservoir in Longdong, Southwest Ordos Basin, China. *Open Geosci.* **2024**, *16*, 20220746. [CrossRef]
24. Morad, S.; Ketzer, J.M.; De Ros, L.F. Spatial and temporal distribution of diagenetic alterations in siliciclastic rocks: Implications for mass transfer in sedimentary basins. *Sedimentology* **2000**, *47*, 95–120. [CrossRef]
25. Lanson, B.; Beaufort, D.; Berger, G. Authigenic kaolin and illitic minerals during burial diagenesis of sandstones: A review. *Clay Miner.* **2002**, *37*, 1–22. [CrossRef]
26. Cai, L.X.; Yang, T.; Tian, J.C.; Yi, J.; Ren, Q. Advances in Development and Growth Mechanisms of Clay Minerals in Tight Sandstones. *Acta Sedimentol. Sin.* **2023**, *41*, 1859–1889.
27. Meng, W.B.; Lü, Z.X.; Feng, M.S. Origin of authigenic illite and its impacts on relatively high-quality tight sandstone reservoirs. *Acta Pet. Sin.* **2011**, *32*, 783–790.
28. Ajdukiewicz, J.M.; Lander, R.H. Sandstone reservoir quality prediction: The state of the art. *AAPG Bull.* **2010**, *94*, 1083–1091. [CrossRef]
29. Worden, R.H.; Morad, S. Clay Minerals in Sandstones: Controls on Formation and Distribution and Evolution. In *Clay Minerals in Sandstones*; Wiley-Blackwell: Hoboken, NJ, USA, 2009.
30. Bloch, S.; Lander, R.H.; Bonnell, L. Anomalously high porosity and permeability in deeply buried sandstone reservoirs: Origin and predictability. *AAPG Bull.* **2002**, *86*, 301–328. [CrossRef]

Disclaimer/Publisher's Note: The statements, opinions and data contained in all publications are solely those of the individual author(s) and contributor(s) and not of MDPI and/or the editor(s). MDPI and/or the editor(s) disclaim responsibility for any injury to people or property resulting from any ideas, methods, instructions or products referred to in the content.